NJC

ROYAL SOCIETY OF CHEMISTRY

PAPER

View Article Online
View Journal | View Issue

Cite this: *New J. Chem.*, 2025, **49**, 2484

Substituent-regulated photophysical properties of 8*a*-methyl-2,3-diphenylindolizin-1(8*aH*)-one derivatives and their application in the detection of bilirubin in blood and urine†

S. Shurooque Kanneth, A. Thoyyiba and Lakshmi Chakkumkumarath *

Received 15th December 2024,
Accepted 17th January 2025

DOI: 10.1039/d4nj05341a

rsc.li/njc

8*a*-Methyl-2,3-diphenylindolizin-1(8*aH*)-one derivatives with electronically diverse substituents at the *para* position of the C-2 and C-3 phenyl rings were synthesized, and their photophysical properties were examined. The electronic effects exerted by the substituents on the C-2 phenyl ring caused a shift in the emission wavelength, whereas the substituents on the C-3 phenyl ring had no impact. One of the derivatives with *p*-nitrophenyl group as the C-2 substituent exhibited intramolecular charge transfer characteristics. The solvent-polarity-dependent emission properties facilitated its application as a sensor for detecting moisture in nonpolar solvents with a lowest detection limit of 0.009%. These compounds also responded to bilirubin with a turn-off response, allowing its detection in blood and urine at submicromolar levels. Emission quenching in the presence of bilirubin was attributed to the primary inner filter effect.

Introduction

N-Heterocyclic scaffolds form the core structure of numerous physiologically active natural products and pharmaceutically significant compounds.[1,2] They are also part of many well-established fluorescent compounds such as BODIPY, cyanines, and pyridine- and indole-based dyes. Their structural diversity and tuneable photophysical properties make them attractive candidates for the development of luminescent materials. N-Fused bicyclic indolizines are part of several biologically relevant molecules and also serve as versatile building blocks in synthesis.[3,4] In addition, indolizine-based fluorophores with applications in sensing and cell imaging have also been reported.[5–15] A popular fluorophore harbouring an indolizine core is 1*H*-pyrrolo-[3,4-β]indolizin-3-one (Seoul-Fluor).[16–19] The emission of Seoul-Fluor can be tuned by introducing various substituents on the heterocyclic core. Owing to their impressive photophysical properties, they have been successfully employed in sensing and lipid droplets imaging.[20] Novel fluorophores have been obtained by structurally modifying the indolizine core with appropriate substituents. For instance, introducing an imidazole unit at the C-7 position resulted in highly emissive indolizine derivatives.[9] The electronic tuning of the indolizine core accomplished through substituent modification resulted in fluorophores having emissions that span the entire visible range.[21] Chalcone-indolizine conjugates exhibited solvatochromism and particle size-dependent emission in the solid state. Indolizine-based solvatochromic dyes, ESIPT fluorophores, metal ion/anion sensors, polarity probes for lipid droplet imaging, crystallochromic dyes, and halochromic molecular switches have been reported.[11,22–28]

Contrary to the conventional perception as a waste byproduct of heme catabolism, the yellow pigment bilirubin has multiple physiological functions in humans.[29,30] Recent studies have indicated that the beneficial role of bilirubin in human physiology ranges from its ability to act as an antioxidant to regulation of the immune system and neuroprotection. Total bilirubin in the serum is made of two components: glucuronic acid-conjugated bilirubin and unconjugated bilirubin. In healthy individuals, total serum bilirubin levels are typically around 17 μM L^{-1}.[31] However, in individuals with hyperbilirubinemia, bilirubin levels exceed 50 μM and even surpass 170 μM in adults and 340 μM in newborns.[32] Critical neonatal hyperbilirubinemia reaching levels above 425 μM poses a risk of bilirubin encephalopathy (kernicterus) in infants.[33] Serum bilirubin serves as an important biomarker of many liver diseases such as hepatitis, autoimmune liver diseases, drug-induced hepatoxicity, and liver cirrhosis.[34] Thus, estimating bilirubin levels is vital to assess liver function, diagnose jaundice, monitor neonatal health, evaluate hemolytic disorders, and assess treatment efficacy in end-stage liver diseases. In routine clinical practice, the Jendrassik–Grof (J–G) method is employed to determine bilirubin levels in the blood serum. This method involves the formation of an azo dye through the reaction of bilirubin with

Department of Chemistry, National Institute of Technology Calicut, Calicut-673601, Kerala, India. E-mail: lakshmic@nitc.ac.in

† Electronic supplementary information (ESI) available. See DOI: https://doi.org/10.1039/d4nj05341a

diazotized sulfanilic acid, resulting in a red color under neutral conditions and a blue color under alkaline conditions.[35] However, the practical application of the J–G method is constrained by potential interference from other heme proteins, high blood lipid levels, and the pH-dependent sensitivity of the diazo reaction.[36] Other drawbacks of this technique include lengthy procedures involving multiple steps, reagents, and the need for skilled technicians. Several alternative methods based on spectroscopic, electrochemical, SERS, and liquid chromatographic techniques have been developed for bilirubin assays.[36,37] Among these, fluorescence-based methods have evolved as potent tools for detecting bilirubin, offering several advantages over traditional techniques such as colorimetric assays or spectrophotometry. They stand out for their superior sensitivity, selectivity, dynamic range, real-time monitoring, and automation compatibility. Fluorescent sensors for bilirubin mainly operate *via* fluorescence resonance energy transfer (FRET), inner filter effect (IFE), and photoinduced electron transfer (PET). Bilirubin detection has been achieved using emissive polymers that can form specific non-covalent interactions with bilirubin. Such interactions facilitate FRET between the probe and bilirubin, leading to analyte-dependent changes in their emission.[38] FRET-based sensing systems have also been developed using emissive small organic molecules, carbon dots, and metal–organic frameworks.[39–43] Bilirubin detection is also achieved *via* the IFE when there is considerable overlap between the absorption spectrum of the sensor and bilirubin.[44,45] Typical examples include fluorescent lanthanide complexes, metallic nanoclusters coated with enzymes, *etc.*[46,47] There have been reports of bilirubin sensors based on methods such as displacement technique, and bilirubin-induced breakdown of metal–organic frame works.[48,49]

Results and discussion

It is well established that the photophysical response of emissive molecules can be modified by introducing substituents with different electronic properties at their periphery. We anticipated that electronic tuning of the indolizinone scaffold could be achieved by introducing electron-donating/electron-withdrawing groups at the *para* position of the C-2 and C-3 phenyl rings. With this objective, ten indolizinone derivatives (**1–10**) were synthesized. The reaction between 4-aryl-2-(pyridin-2-yl)but-3-yn-2-ols and suitably substituted iodo-/bromobenzene in the presence of a Pd catalyst yielded compounds **1–10** in moderate yields (Scheme 1). All compounds were characterized using ^{1}H NMR, ^{13}C NMR, and HRMS. The geometry optimization of compounds **1–5**, **7**, and **9** was performed in the gas phase using quantum mechanical calculations at the M06/def2-TZVPP//BP86/def2-SVP level of theory. The aryl substituents at the C-2 position were tilted from the indolizinone plane, with dihedral angles ranging from 25° to 33° (Fig. 1 and Fig. S1, S2, ESI†). The unsubstituted derivative **1** shows a dihedral angle of 30.09°, whereas the C-2 substituted derivatives **2–5**, it is in the range of 27°–25°, with the nitro derivative **3** showing the lowest angle of 25.48°. The aryl substituents at C-3 were tilted from the plane of the indolizinone ring, with a dihedral angle of 58°–61°.

Photophysical properties

The absorption spectra of compounds **1–10** were recorded in solvents of different polarities. All the compounds exhibited broad absorption peaks with $\lambda_{ab.max}$ in the range of 420–440 nm. Polarity-dependent variations in the absorption wavelength were not observed in any of the cases, suggesting a nonpolar ground state. Similarly, the emission wavelengths of all compounds, except compound **3**, were unaffected by variations in solvent polarity, indicating the absence of intramolecular charge transfer. However, the $\lambda_{em.max}$ values of these compounds varied depending on the electronic nature of the substituents and whether they were on the C-2 or C-3 phenyl rings. Compound **1**, with unsubstituted C-2 and C-3 phenyl rings, exhibited a weak emission ($\lambda_{em.max}$ = ~488 nm) in different solvents. The introduction of an electron-releasing methoxy group on the C-2 phenyl ring (compound **2**) pushed the emission to a longer wavelength (538 nm) and resulted in a higher quantum yield (1.7–5.3%) (Fig. 2, Fig. S3–S12 and Table 1, Table S1, ESI†). The solution

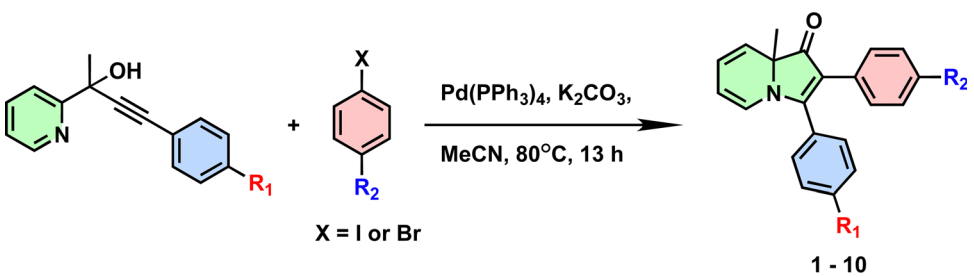

1: X = I, R_1 = H; R_2 = H (37%)
2: X = Br, R_1 = H; R_2 = OCH_3 (32%)
3: X = Br, R_1 = H; R_2 = NO_2 (40%)
4: X = Br, R_1 = H; R_2 = Br (35%)
5: X = Br, R_1 = H; R_2 = CHO (46%)
6: X = Br, R_1 = H; R_2 = $OC_{18}H_{37}$ (42%)
7: X = Br, R_1 = OCH_3; R_2 = H (32%)
8: X = Br, R_1 = $OC_{18}H_{37}$; R_2 = H (28%)
9: X = Br, R_1 = OCH_3; R_2 = OCH_3 (29%)
10: X = Br, R_1 = $OC_{18}H_{37}$; R_2 = $OC_{18}H_{37}$ (28%)

Scheme 1 Synthesis of indolizinone derivatives **1–10**. Isolated yields are given in parenthesis.

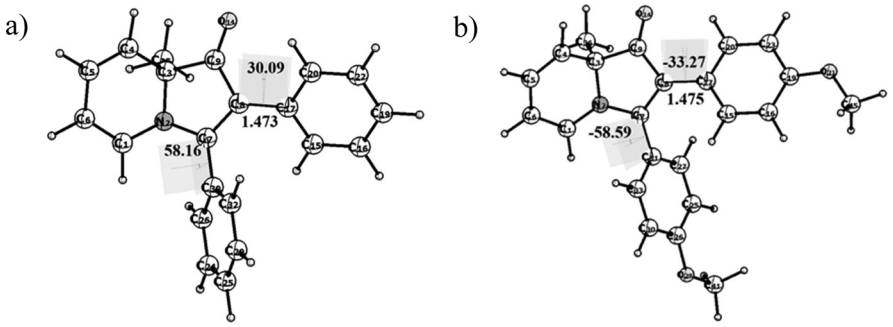

Fig. 1 Optimized geometries of (a) **1** and (b) **9** at BP86/def2-SVP level of theory in the gas phase. All angles are given in degrees and bond lengths in Å.

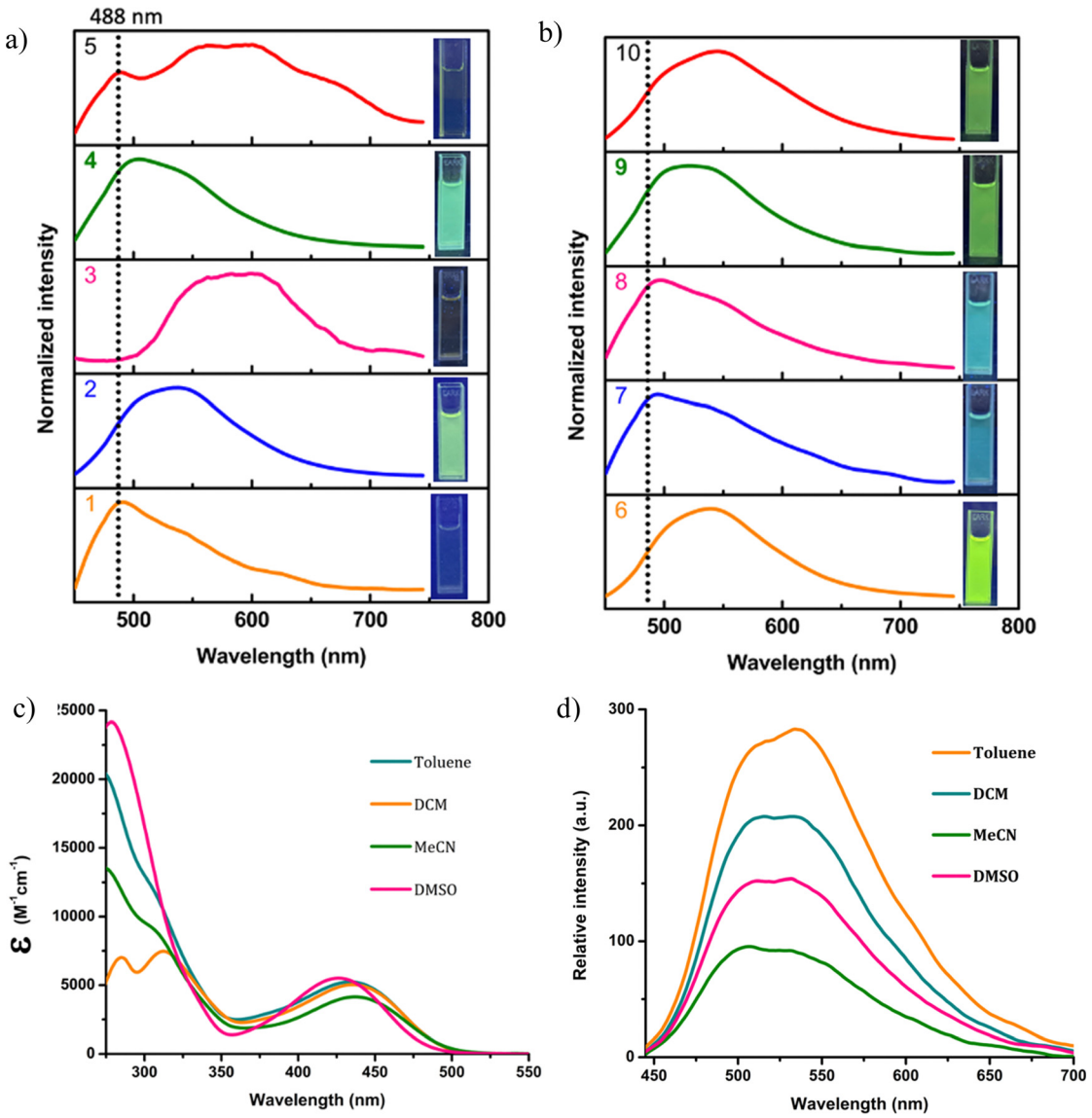

Fig. 2 (a) and (b) Emission spectra of the 33 μM solution of compounds **1–10** in DMSO and their photographs under 365 nm UV lamp; (c) absorption and (d) emission spectra of 33 μM solution of 9 in different solvents.

appeared green when viewed under a 365 nm UV lamp. Compound **6**, with an octadecyloxy group on the C-2 phenyl ring, exhibited emission in the same range, but with a higher quantum yield of 6.7–9.8%, the highest among the series. Replacing the –OMe group with bromine (compound **4**) shifted the emission maximum to 504 nm and 503 nm in toluene and DMSO,

Table 1 Photophysical properties of compounds **1–10** in DMSO

Compound	λ_{ab} (nm)	ε (M^{-1} cm^{-1})	λ_{em} (nm)	Quantum yield[a] (%)	Lifetime[b] (ns)	k_r[c] (10^7 s^{-1})	Σk_{nr}[c] (10^8 s^{-1})
1	431	6630	488	—	—	—	—
2	436	2760	492, 538	2.9	4.6	0.6	2.1
3	435	11 600	569	—	—	—	—
4	429	5430	503, 535	1.8	3.5	0.5	2.8
5	433	9870	482, 586	—	—	—	—
6	383, 436	2490	539	9.3	6.1	1.5	1.4
7	432	4500	492, 543	0.26	3.3	0.1	3.0
8	431	4890	495, 544	1.1	3.6	0.3	2.8
9	426	5450	509, 534	5.6	5.4	1.0	1.8
10	438	4950	545	5.0	6.3	0.8	1.5

[a] Quantum yield in solution was calculated using equation $\Phi = \Phi_R (I/I_R) (OD_R/OD) (n^2/n_R^2)$, where Φ is the emission quantum yield, I the integrated emission intensity, OD the optical density, n the refractive index, and the subscript R refers to the reference fluorophore of known quantum yield. Fluorescein in 0.1 M NaOH (Q.Y = 0.79) was used as the standard.[50] [b] The average lifetime τ was calculated by using equation $\tau = \Sigma(\alpha_i\tau_i^2)/\Sigma(\alpha_i\tau_i)$, where α_i is the amplitude of the lifetime component and τ_i is the respective lifetime value. [c] Radiative (k_r) and non-radiative (Σk_{nr}) rate constants estimated using the approximation that the emissive state is formed with unitary efficiency and thus $k_r = \Phi/\tau$ and $\Sigma k_{nr} = (1 - \Phi)/\tau$.

respectively, with quantum yields ranging from 0.49–1.8%. Compound **3**, with a nitro substituent, exhibited very weak emission in polar solvents; however, its solutions in nonpolar solvents were emissive. $\lambda_{em.max}$ appeared at 496 nm and 569 nm in toluene and dichloromethane, respectively, and the corresponding quantum yields were 4.0% and 3.7%. The polarity-dependent redshift suggests an intramolecular charge transfer in the excited state. Irrespective of the solvent polarity, compound **5** with a –CHO group, was also weakly emissive. The emission of compounds **7** and **8** with methoxy and octadecyloxy groups at the *para* position of the C-3 phenyl ring appeared at 493 nm and 497 nm in toluene, respectively, which was closer to the emission wavelength of compound **1**. When the –OMe group was introduced on both the C-2 and C-3 phenyl rings (compound **9**), emission appeared in the green region with $\lambda_{em.max}$ similar to compound **2**. However, the quantum yields in DCM, acetonitrile, and DMSO were higher than that of compound **2**. The photophysical response of the corresponding octadecyl derivative **10** was similar to compound **6**. In summary, both the electron-donating and electron-withdrawing groups on the C-2 phenyl ring shifted the emission bathochromically compared to the parent compound **1**. However, the substitution on the C-3 phenyl ring exerted minimum electronic effects, as evidenced by the marginal shift in the emission wavelength compared to the parent compound **1**. The viscosity-dependent emission of selected compounds **1**, **4**, and **8** were studied by recording their emission spectra in glycerol/MeOH mixtures (Fig. S13, ESI†). A noticeable enhancement in emission intensity was observed upon increasing the percentage of glycerol, resulting in a 9-, 5-, and 2-fold increase for compounds **1**, **4**, and **8**, respectively. The increase in intensity without changes in $\lambda_{em.max.}$ could be due to the slowing down of intramolecular rotations in viscous environments, which deactivates nonradiative decay pathways.

TD-DFT analysis

The nature of the electronic transitions in the indolizinone derivatives in DMSO was further analyzed by TD-DFT calculations using the B3LYP/6-31G(d) method. The electronic transition energies and corresponding oscillator strengths are listed in Table S2 (ESI†) and shown in Fig. 3 and Fig. S14 (ESI†). In all cases, the electronic transition with the highest oscillator strength (f) originates mainly from the highest occupied molecular orbital (HOMO) to the lowest unoccupied molecular orbital (LUMO). The occupied orbitals of all the compounds were located on the indolizinone unit and the C-2 aryl fragment, with no contribution from the C-3 aryl fragment.

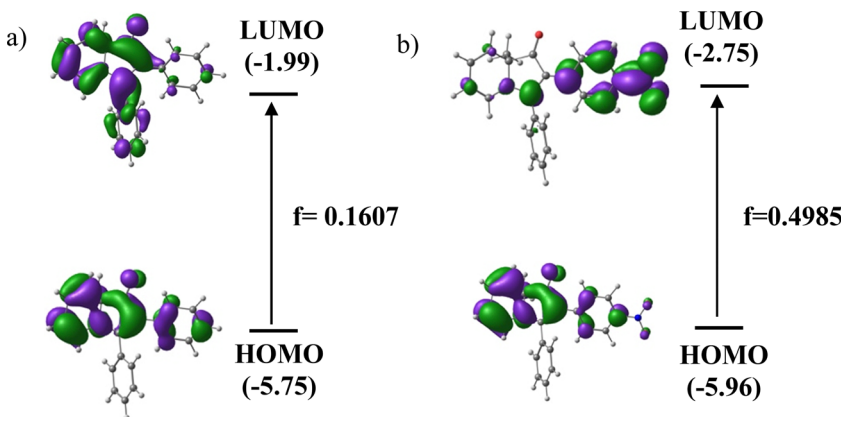

Fig. 3 Important electronic transitions and the corresponding molecular orbitals in (a) **1** and (b) **3** computed using TD-DFT at M06/def2-TZVPP//BP86/def2-SVP level of theory in DMSO. Eigenvalues are given in eV in parenthesis.

However, except for **3** and **5**, the LUMOs of the compounds were primarily located on the indolizinone ring and the C3 aryl fragment. In the case of compounds **3** and **5**, where the substituents are electron-withdrawing (–CHO and $–NO_2$), the LUMO has a major contribution from the C-2 aryl unit. The electronic transitions in these two compounds seem to involve intramolecular charge transfer from the indolizinone unit to the C-2 aryl unit.

Polarity-dependent emission of compound 3 and its application in monitoring water content in nonpolar organic solvents

Compound **3** exhibited intense emission in nonpolar solvents such as toluene and dichloromethane, but was non-emissive in polar solvents such as MeCN and DMSO (Fig. 4a). It also showed positive solvatochromic behaviour. For instance, its emission appeared at 496 nm in toluene, which was red-shifted to 569 nm in DMSO. The changes in emission intensity with change in the solvent polarity were further validated by recording the emission spectra in toluene with increasing percentages of methanol. The addition of 10% methanol resulted in 85% emission quenching (Fig. 4b and c). This observation prompted us to explore the feasibility of using this compound for the detection of water in nonpolar solvents. Incremental amounts of water were added to a solution of compound **3** in 1,4-dioxane, and emission spectra were recorded after each addition (Fig. 5). A gradual decrease in the emission intensity was observed with increasing concentrations of water (0–3%). The calibration plot obtained by plotting the emission intensity against the percentage of water showed a linear response in the range of 0–1% water. The lowest detection limit (LoD) was calculated using the equation 3σ/slope, where σ is the standard deviation of 10 blank measurements, and LoD was estimated to be 0.009%. The emission quenching with an increase in solvent polarity can be due to the ICT characteristics of the compound **3**. Increased polarity of the medium facilitates ICT and such charge transfer complexes are either weakly or non-emissive in polar environments.

Bilirubin detection

The IFE is regarded as an undesirable phenomenon in fluorescence measurements. However, recent investigations have illustrated its utility in the detection and quantification of several analytes. The primary advantage of IFE-based probes is their ability to convert conventional colorimetric protocols into fluorescence sensing. This effectively addresses the intrinsic limitations of colorimetric methods, including their low detection sensitivity, inadequate repeatability, and complex interference factors. Moreover, the detection process does not require direct interaction between the probe and the analyte. The primary IFE (pIFE) occurs when there is a spectral overlap between the excitation spectra of the fluorophore and absorption spectra of the analyte, resulting in competitive absorption.

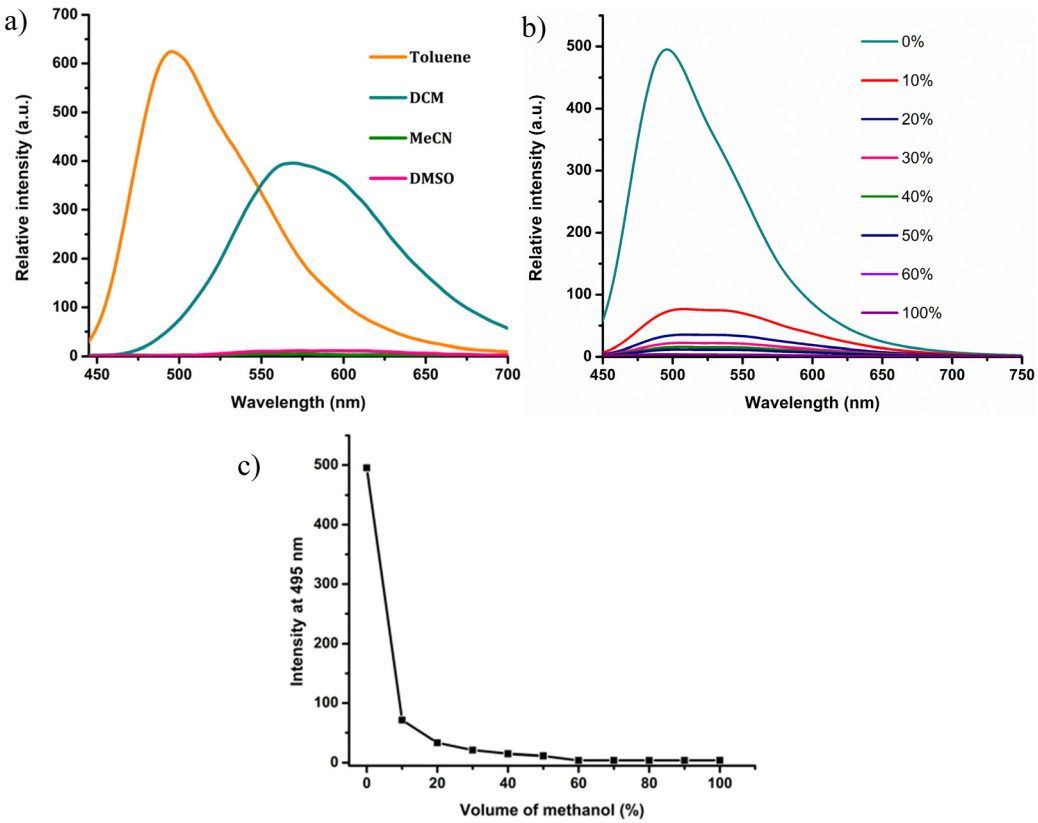

Fig. 4 Fluorescence spectra of 33 μM solution of **3** (a) in different solvents, (b) in toluene in the presence of varying percentages of methanol, and (c) plot of percentage of methanol *vs.* emission intensity at 495 nm.

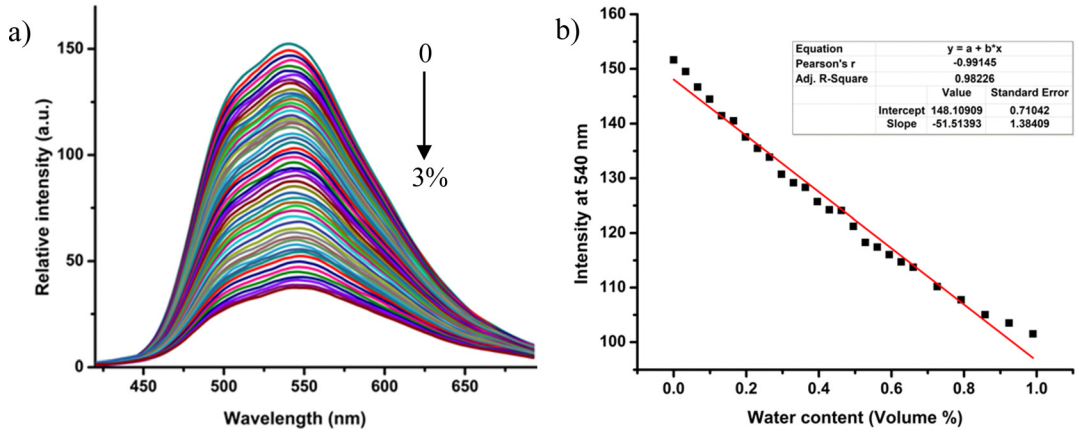

Fig. 5 (a) Fluorescence spectra of 33 μM solution of **3** in 1,4-dioxane with increasing percentage of water (0–3%) and (b) the corresponding calibration plot.

Bilirubin exhibits strong absorption between 400 nm and 500 nm, with a molar absorption coefficient (ε) of 53 846 cm^{-1} M^{-1}. Indolizinone derivatives **1–10** also absorb in this range. Fig. 6a and Fig. S15 (ESI†) show the overlap between the absorption/emission spectra of compound **9** and the absorption spectra of bilirubin. The significant overlap between the absorption spectra of bilirubin and the excitation spectra of indolizinones indicates the possibility of pIFE. Therefore, we evaluated the feasibility of using these compounds for the detection of bilirubin. Compounds **2**, **6**, **9**, and **10** showed relatively higher quantum yields than other compounds in DMSO, and hence they were selected for bilirubin detection studies.

The response of compounds **2**, **6**, **9**, and **10** to bilirubin was then evaluated by mixing DMSO solutions with 5 eq. of bilirubin. The addition of bilirubin resulted in instantaneous fluorescence quenching. To assess the potential interference from other analytes, we repeated the experiment by adding 5 eq. of interfering species (Fig. 6b and Fig. S16, ESI†). These studies demonstrate that these compounds are highly selective for bilirubin.

The changes in the emission spectra of compounds **2**, **6**, **9**, and **10** with increasing amounts of bilirubin were then examined. The incremental addition of bilirubin to a 33 μM solution resulted in a gradual decrease in emission without any band shift (Fig. 7 and Fig. S17–S19, ESI†). For instance, the emission of compound **2** was quenched by 16.5% and 69% upon the addition of 0.1 eq. and 1 eq. of bilirubin, respectively. Maximum quenching of 97.1% was achieved with the addition of 5 eq. of bilirubin. All four probes exhibited a linear response in the range 0–0.3 equivalents of bilirubin. Beyond this, the response followed an exponential fit, indicating the presence of IFE. The LoD values were estimated as 0.12 μM, 0.08 μM, 0.09 μM, and 0.3 μM for probes **2**, **6**, **9**, and **10**, respectively. One of the major advantages of IFE-based probes is their short response time. We examined the response time of the compounds to bilirubin and found that a stable signal was achieved within 10 seconds (Fig. S20, ESI†).

Real sample analysis

All experiments on serum and urine were performed in accordance with the guidelines of the National Institute of Technology Calicut and approved by the ethics committee at the National Institute of Technology Calicut. Informed consent was obtained from human participants of this study. The quantification of bilirubin in complex biological fluids was subsequently attempted by employing the 'spike-recovery

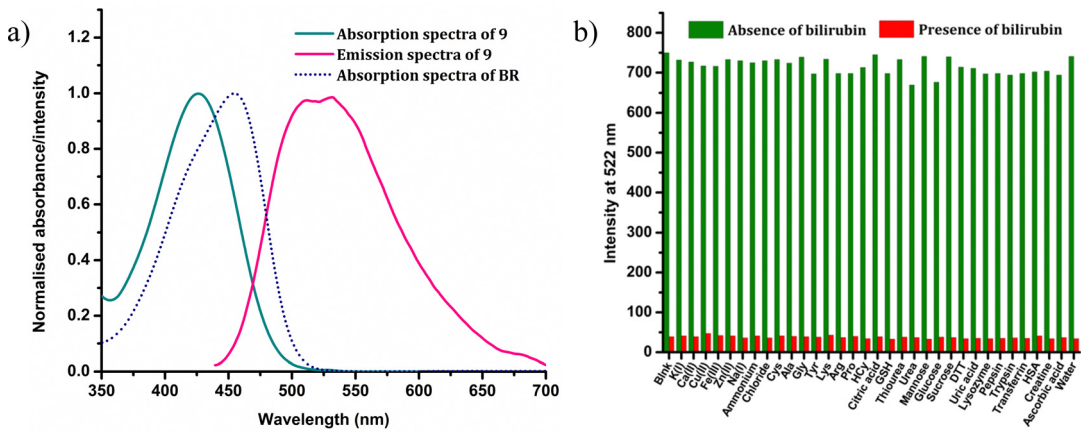

Fig. 6 (a) Normalised absorption and emission spectra of 33 μM solution of **9** along with the normalized absorption spectra of bilirubin (BR) in DMSO. (b) Fluorescence response of 33.33 μM solution of **9** on addition of 5 eq. (166 μM) of various analytes in the absence (green) and presence (red) of 5 eq. of bilirubin in DMSO.

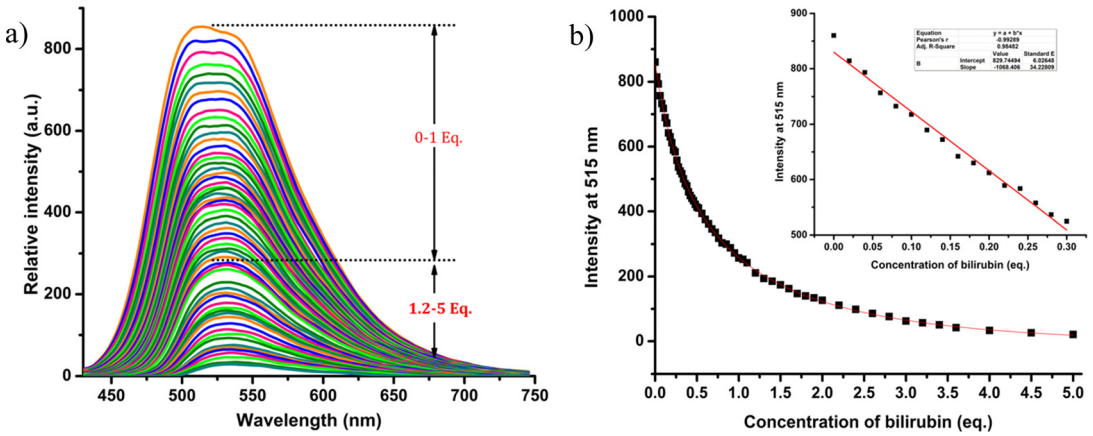

Fig. 7 (a) Emission spectra of 33 μM solution of **9** in the presence of an increasing concentration of bilirubin in DMSO (λ_{ex} = 430 nm); (b) the plot of bilirubin concentration *versus* emission intensity at 538 nm (inset: The linear range).

approach' using compound **6**. Blood samples were collected from the NITC health center in 4 mL clot activator vacutainer tubes, allowed to clot, and then centrifuged at 2000 rpm for 5 minutes. The resulting serum supernatant was collected and immediately used for analysis. The concentration of bilirubin in the serum was determined using a modified Jendrassik & Grof method from a clinical laboratory ([bilirubin] = 3.4 μM). For the analysis, 0.1 mL of serum was added to 2.9 mL of DMSO and spiked with bilirubin solutions of concentrations 3.33 μM, 6.66 μM, and 9.99 μM. Additionally, 10 μL of a 10 mM stock solution of compound **6** was added to each sample and the emission spectra were recorded. Standard solutions of bilirubin (3.33 μM, 6.66 μM, and 9.99 μM) were also prepared without serum, and compound **6** was added to this before recording the emission spectra. Bilirubin concentrations in the serum samples were calculated using the equation $C_{BR}/C_{STD} = F/F_{STD}$, where C_{BR} and C_{STD} are the bilirubin concentrations in the unknown and standard samples, respectively, and F and F_{STD} are the corresponding fluorescence intensities after adding a specific volume of serum from the unknown and standard samples. The bilirubin concentration determined using the spike recovery method closely matched the actual value, with recovery rates ranging from 97% to 101% (Table 2). Similarly, urine samples were obtained from a healthy individual and verified for the absence of bilirubin using clinical tests. The samples were then diluted 30 times with DMSO and spiked with bilirubin solutions (concentrations: 3.33 μM, 6.66 μM, and 9.99 μM), and the emission spectra were recorded. Bilirubin concentrations were then calculated employing the same method used for serum analysis. The bilirubin concentrations were determined to be 3.29 μM, 6.7 μM, and 10.1 μM, which closely matched the actual values. A summary of the analysis results is presented in Table 2.

Table 2 Determination of bilirubin in blood and urine sample

Sample	Concentration of bilirubin (μM) (by modified Jendrassik & Grof's method)	Bilirubin added (μM)	Bilirubin found (μM)	RSD (%)	Recovery (%)
Blood	0.11	3.33	3.36	1.72	97.5
		6.66	6.68	1.2	98.6
		9.99	10.18	1.91	100.8
Urine	0	3.33	3.29	3.07	98.7
		6.66	6.7	1.4	100.6
		9.99	10.1	2.77	101.1

Conclusion

In summary, 8*a*-methyl-2,3-diphenylindolizin-1(8*aH*)-one derivatives having electronically diverse substituents at the *para* position of C-2 and C-3 phenyl rings were prepared and characterized. All the compounds exhibited substituent-dependent photophysical properties. Electron-donating or electron-withdrawing groups on the C-2 phenyl ring resulted in a redshift of the emission compared to the parent compound **1**. However, their emission was found to be less influenced by the substituents on the C-3 phenyl ring. The difference in the electronic tuning can be attributed to the higher dihedral angle between the planes of C-3 phenyl and indolizinone core. Among these compounds, compound **3** with a nitro group on the C-2 phenyl ring exhibited intramolecular charge transfer characteristics in its emission. It displayed intense emission in nonpolar solvents, whereas substantial emission quenching occurred in polar solvents. Consequently, compound **3** was utilized to evaluate moisture content in nonpolar solvents. Since the excitation spectra of indolizinone derivatives overlapped with the absorption spectrum of bilirubin, they were successfully used for the quantitative estimation of bilirubin in blood and urine. The detection relied upon the pIFE and LoD was found to be in the submicromolar levels.

Author contributions

S. S. K.: synthesis, characterization, photophysical studies, data analysis, manuscript preparation; T. A.: synthesis, characterization, photophysical studies: L. C.: conceptualization, supervision, data analysis, manuscript preparation, review and editing.

Data availability

The data supporting this article have been included as part of the ESI.†

Conflicts of interest

The authors declare no competing financial interest.

Acknowledgements

The authors thank DST-FIST for the HRMS facility at NIT Calicut, and the Centre for Materials Characterization (CMC)-NIT Calicut for the NMR facility. We also thank SAIF, MG University, Kottayam for fluorescence lifetime measurements. S. S. K thanks CSIR for the fellowship.

References

1 O. Ebenezer, M. A. Jordaan, G. Carena, T. Bono, M. Shapi and J. A. Tuszynski, *Int. J. Mol. Sci.*, 2022, **23**, 8117.
2 A. Mermer, T. Keles and Y. Sirin, *Bioorg. Chem.*, 2021, **114**, 105076.
3 B. Sadowski, J. Klajn and D. T. Gryko, *Org. Biomol. Chem.*, 2016, **14**, 7804–7828.
4 A. A. Nevskaya, A. D. Zinoveva, E. V. Van der Eycken and L. G. Voskressensky, *Asian J. Org. Chem.*, 2023, **12**, e202300359.
5 J. Sung, Y. Lee, J. H. Cha, S. B. Park and E. Kim, *Dyes Pigm.*, 2017, **145**, 461–468.
6 V. Arun, S. K. Choi, J. H. Han, H. Choi, H. M. Kim, W. Kim, J. Choi, J. Kim and E. Kim, *Dyes Pigm.*, 2022, **200**, 110118.
7 H. Kim, S. Lee, K. W. Lee, E. S. Kim, H. M. Kim, H. Im, H. C. Yoon, J. G. Ko and E. Kim, *Dyes Pigm.*, 2023, **215**, 111287.
8 M. M. Vieira, B. T. Dalberto, N. B. Padilha, H. C. S. Junior, F. S. Rodembusch and P. H. Schneider, *Dyes Pigm.*, 2023, **216**, 111332.
9 R. Sarkar, T. Chaudhuri, A. Karmakar and C. Mukhopadhyay, *Org. Biomol. Chem.*, 2015, **13**, 11674–11686.
10 R. Cui, Y. Gao, H. Ge, G. Shi, Y. Li, H. Liu, C. Ma, Y. Ge and C. Liu, *New J. Chem.*, 2022, **46**, 8088–8093.
11 D. Maiti, S. Munan, S. Singh, R. Das, A. Samanta and S. Sen, *J. Mater. Chem. B*, 2023, **11**, 2191–2199.
12 J. S. A. Badaro, A. Wrzosek, O. Morawski, A. Szewczyk, I. Deperasińska and D. T. Gryko, *Org. Chem. Front.*, 2024, **11**, 6627–6641.
13 J. Gayton, S. A. Autry, W. Meador, S. R. Parkin, G. A. Hill, N. I. Hammer and J. H. Delcamp, *J. Org. Chem.*, 2019, **84**, 687–697.
14 T. Kim and J. Kim, *Molecules*, 2022, **27**, 1–15.
15 S. Yi, D. Kim, W. Cho, J. H. Lee, J. H. Kwon, J. Kim and S. B. Park, *JACS Au*, 2024, **4**, 2896–2906.
16 E. Kim, S. Lee and S. B. Park, *Chem. Commun.*, 2011, **47**, 7734–7736.
17 E. Kim, S. Lee and S. B. Park, *Chem. Commun.*, 2012, **48**, 2331–2333.
18 Y. Lee, S. Na, S. Lee, N. L. Jeon and S. B. Park, *Mol. BioSyst.*, 2013, **9**, 952–956.
19 E. Kim, M. Koh, B. J. Lim and S. B. Park, *J. Am. Chem. Soc.*, 2011, **133**, 6642–6649.
20 E. Kim, Y. Lee, S. Lee and S. B. Park, *Acc. Chem. Res.*, 2015, **48**, 538–547.
21 B. Liu, Z. Wang, N. Wu, M. Li, J. You and J. Lan, *Chem. – Eur. J.*, 2012, **18**, 1599–1603.
22 M. J. Albaladejo, M. J. González-Soria and F. Alonso, *Green Chem.*, 2018, **20**, 701–712.
23 A. J. Stasyuk, M. Banasiewicz, B. Ventura, M. K. Cyrański and D. T. Gryko, *New J. Chem.*, 2014, **38**, 189–197.
24 R. Ji, A. Liu, S. Shen, X. Cao, F. Li and Y. Ge, *RSC Adv.*, 2017, **7**, 40829–40833.
25 R. Cui, Y. Gao, H. Ge, G. Shi, Y. Li, H. Liu, C. Ma, Y. Ge and C. Liu, *New J. Chem.*, 2022, **46**, 8088–8093.
26 C. Dohmen, H. Ihmels, R. Kreienmeier and B. O. Patrick, *Chem. Commun.*, 2019, **55**, 11071–11074.
27 Y. Zhang, J. Garcia-Amorós, B. Captain and F. M. Raymo, *J. Mater. Chem. C*, 2016, **4**, 2744–2747.
28 T. Antón-Cánovas, S. Achelle, M. Paz Fernández-Liencres, A. Navarro, F. Alonso and J. Rodríguez-López, *J. Mol. Liq.*, 2023, **380**, 121758.
29 L. Vitek, T. D. Hinds, D. E. Stec and C. Tiribelli, *Trends Mol. Med.*, 2023, **29**, 315–328.
30 L. Vítek and C. Tiribelli, *J. Hepatol.*, 2021, **75**, 1485–1490.
31 N. Guirguis, A. X. Bertrand, C. F. Rose and S. Matoori, *Adv. Healthcare Mater.*, 2023, **12**, 1–8.
32 J. P. Ndabakuranye, S. Li, G. Burchall, K. Fox, T. Piva, Z. Xu, O. Kavehei, S. Prawer and A. Ahnood, *Sens. Diagn.*, 2022, **1**, 932–954.
33 T. W. R. Hansen, R. J. Wong and D. K. Stevenson, *Physiol. Rev.*, 2020, **100**, 1291–1346.
34 M. M. Ramírez-Mejía, S. M. Castillo-Castañeda, S. C. Pal, X. Qi and N. Méndez-Sánchez, *J. Clin. Transl. Hepatol.*, 2024, **12**, 939–948.
35 A. G. Cherian, S. J. Soldin and J. G. Hill, *Clin. Chem.*, 1981, **27**, 748–752.
36 V. Narwal, B. Batra, V. Kalra, R. Jalandra, J. Ahlawat, R. Hooda, M. Sharma and J. S. Rana, *Sens. Bio-Sensing Res.*, 2021, **33**, 100436.
37 R. Rawal, P. R. Kharangarh, S. Dawra, M. Tomar, V. Gupta and C. S. Pundir, *Process Biochem.*, 2020, **89**, 165–174.
38 T. Senthilkumar and S. K. Asha, *Macromolecules*, 2015, **48**, 3449–3461.
39 S. Ellairaja, K. Shenbagavalli, S. Ponmariappan and V. S. Vasantha, *Biosens. Bioelectron.*, 2017, **91**, 82–88.
40 T. Senthilkumar and S. K. Asha, *Macromolecules*, 2013, **46**, 2159–2171.
41 Y. Guo, C. Wei, R. Wang and Y. Xiang, *Anal. Biochem.*, 2023, **666**, 115078.
42 M. A. Chanu, S. Mondal, N. Zehra, A. S. Tanwar and P. K. Iyer, *ACS Appl. Polym. Mater.*, 2022, **4**, 3491–3497.
43 K. Yi, H. Li, X. Zhang and L. Zhang, *Inorg. Chem.*, 2021, **60**, 3172–3180.
44 K. Sasikumar, R. Rajamanikandan and H. Ju, *J. Sci. Adv. Mater. Devices*, 2023, **8**, 100599.

45 C. Pan, X. Qin, M. Lu and Q. Ma, *Anal. Methods*, 2023, **15**, 3034–3042.
46 A. Q. He, Q. Li, Z. Q. Yu, J. Tian, J. Song, J. Feng, Y. Z. Xu, I. Noda and Y. Ozaki, *Spectrochim. Acta, Part A*, 2021, **251**, 119427.
47 M. K. Abraham, K. Gouri Krishna, A. S. Madanan, S. Varghese, A. Ibrahim Shkhair, G. Indongo, G. Rajeevan, N. S. Vijila, B. K. Arathy and S. George, *J. Photochem. Photobiol., A*, 2024, **449**, 115424.
48 N. Singla, M. Ahmad, V. Mahajan, P. Singh and S. Kumar, *Sens. Diagn.*, 2023, **2**, 1574–1584.
49 M. Xia, Y. Sui, Y. Guo and Y. Zhang, *Analyst*, 2021, **146**, 904–910.
50 A. M. Brouwer, *Pure Appl. Chem.*, 2011, **83**, 2213–2228.

